Electronic Supplementary Information (ESI)

Multi-stimuli responsive conductive sonometallogel: a mechanistic insight into role of ultrasound in gelation

Vinay Kumar Pandey,[a] Manish Kumar Dixit,[a] Sébastien Manneville,[b] Christophe Bucher,[c] and Mrigendra Dubey*[a]

[a]*Department of Chemistry, Indian Institute of Technology (Banaras Hindu University), Varanasi- 221 005, U.P., India.*

[b]*Université de Lyon, ENS de Lyon, Univ Claude Bernard, CNRS Laboratoire de Physique, F-69342 Lyon, France.*

[c]*Univ Lyon, Ens de Lyon, CNRS UMR 5182, Université Claude Bernard Lyon 1, Laboratoire de Chimie, F69342, Lyon, France*

Email: mrigendradubey@gmail.com, mdubey.chy@itbhu.ac.in

Table of Contents **Pages**

General information and experimental methods

Common reagents and solvents were purchased from Merck, Qualigens or S. D. Fine Chem. Ltd, Mumbai, India and used as received. All solvents were purified and dried by standard procedures prior to their use. Triethyl Citrate, 2-hydroxybenzaldehyde and 4-hydroxybenzaldehyde were purchased from Avra synthesis Pvt. Ltd. Hyderabad or Spectrochem Pvt. Ltd. Mumbai, India and used as received.

Sonication experiment was performed on a Selec 1.5 L 50Hz/DTC (16.0 Watt, 33 ± 3 KHz) sonicator. Elemental analyses for carbon, hydrogen and nitrogen were acquired on an Exeter CHN Analyzer CE-440. FT-IR and electronic absorption spectra were obtained on a PerkinElmer Spectrum 100 and Thermo scientific EVOLUTION 201 spectrophotometers, respectively. Photoluminescence spectra were acquired on a Perkin Elmer LS 55 spectrophotometer. The lifetime measurements were made using a TCSPC system from Horiba Yovin (Model: Fluorocube-01-NL). The samples were excited at 378 nm using a picosecond diode laser (Model: Pico Brite-375L) and data analysis was performed using IBH DAS (version 6, HORIBA Scientific, Edison, NJ) decay analysis software. ^{1}H NMR spectra were obtained on a Bruker AVANCE III HD 500 spectrometer. Electrospray ionization mass (ESI-MS) spectra were recorded on a Waters (Micromass MS Technologies) QTof Premier. Thermal Gravimetric analysis data was acquired on a NETZSCH STA 449 F3 at a heating rate of 5 °C min^{-1} under a nitrogen atmosphere. TEM images and AFM were captured using a JEOL JEM 2100 and NT-MDT NTEGRA PRIMA, respectively. Powder XRD data was collected on Rigaku MiniFlex 600 Detector D-tex ultra between angle 2θ = 5-80°. Solution electrical conductivity was measured on a Eutech Instruments CON 5/TDS 5 Conductivity Meter.

The instrument was calibrated with standard solution. Rheology of sonometallogel was performed on Anton Paar MCR 702 Twin Drive Rheometer. Impedance measurements have been carried out with a Biologic® ESP 300 potentiostat equipped with a built-in computer-controlled Frequency Response Analyzer (FRA).

Calibration of ultrasonic bath: Low power continuous ultrasonic waves irradiated for gelation at constant frequency of 33 kHz. The power of ultrasonic waves was calibrated using standard calibration procedure. A known volume of water (20 mL) taken in reaction vessel and it subjected to ultrasonic irradiation for a known time. A graph between time and temperature plotted and with the help of slope of time-temperature plot, power of ultrasonic source was determined using the following equations-

$$dQ= m.c_p.dT$$

Where c_p is heat capacity of water (4.2 J/g)

OR

$$dQ/dt= m.c_p.dT/dt$$

OR

$$Power= m.c_p.dT/dt$$

Thus, the acoustic power of ultrasonic bath calculated and found to be **16.0 Watt** for water sample.
Note: Calibration of ultrasonic bath repeated in triplicate for water samples fixed in middle of bath.

Rheological Study: Measurements were performed using a stress-controlled rheometer (Anton Paar MCR 702 TwinDrive) equipped with stainless steel parallel plates (20 mm diameter, 0.5 mm gap). Experiments were carried out on freshly prepared gels (0.6 % w/v). Linear viscoelastic regions of the samples were determined by measuring the storage modulus, G' (associated with energy storage), and the loss modulus G'' (associated with the loss of energy) as a function of the stress amplitude. Dynamic oscillatory work was kept at a frequency of 0.01 rad s^{-1}. The following tests were performed: increasing amplitude of oscillation up to 100% apparent strain on shear, time and frequency sweeps at 25 °C (~28 min and from 0.01 to 100 rad s^{-1}, respectively), and a heating run to 160 °C at a scan rate of 5 °C min^{-1}. All these measurements were conducted in duplicate.

Conductance Study: Impedance measurements have been carried out with a Biologic® ESP 300 potentiostat equipped with a built-in computer controlled Frequency Response Analyser (FRA) operating over a frequency range of 10 µHz up to 7 MHZ. Home-made one-compartment, two-electrode cells allowing to position two identical cofacially oriented stainless steel or platinum electrodes at a fixed distance has been used to estimate the conductivity of each sample. Variable temperature measurement of the conductivity have been carried out in a home-made jacketed glass cell incorporating two platinum electrodes (Ø = 1cm). The temperature in the cell was controlled with a Lauda-Brinkman RE 104 thermostat. Electrical impedance measurements have been performed in a potentiostatic regime at *EoC*

between 1Hz and 2.5MHz using a maximum voltage of 0.01V. Fitting the experimental Nyquist impedance diagrams (–Im(Z) vs. Re(Z)) was achieved with Z-fit using equivalent electrical circuits involving the actual resistance of the sample R_1, a capacitance C_1 and a constant-phase element Q_1. Such fitting allowed to estimate the resistance of each samples corresponding to the intersection of the curve with the real part of the impedance. The conductivity was calculated from the electrolyte resistance (R_1) using the equation:

$$\sigma = \ell / R\kappa \qquad (1)$$

Where κ is the conductivity in $S.m^{-1}$, R is the ohmic resistance of the electrolyte, ℓ is the distance between the two electrodes (m) and S is the area of the electrodes (m^2). The cell constant, (ℓ/S) was determined at 25°C by calibration with *standard* 0.01D and 0.1D KCl *solutions* having known *conductivity* values, (1408 $\mu S.m^{-1}$, 1285 $mS.m^{-1}$ and 11.13 $S.m^{-1}$).

Synthesis and characterization

Synthesis of CAHN: The precursor compound citric hydrazone was synthesized by mixing the triethyl citrate (0.200 g, 0.74 mmol) and hydrazine hydrate (0.150 g, 2.97 mmol) in methanol (20 mL) at constant stirring for 20 min. The resulting solution was refluxed for additional 6 hours. Upon cooling to room temperature, it afforded a white crystalline powder which was isolated by filtration, washed with diethyl ether and dried in vacuum desiccators. Yield 0.145 g (85%). ^{1}H-NMR (500 MHz, [D_6]DMSO, 25 °C): δ = 9.08 (s, 2 H); 8.88 (s, 1 H); 6.14 (s, 1 H); 4.16 (d, 6 H); 2.47-2.42 (m, 4 H). IR (KBr): $\upsilon(NH_2)_{sym}$ 3357, $\upsilon(NH)_{sym}$ 3292, υ(C=O) 1662 (s).

Synthesis of Isomer 1: The precursor compound CAHN (0.200 g, 0.85 mmol) was dissolved in 2 mL water and then mixed with 20 mL methanol to obtain the clear solution. Methanolic solution (5 mL) of 2-hydroxybenzaldehyde (0.313 g, 2.56 mmol) was added drop wise to CAHN solution and resulting solution stirred for additional 3 hours. It afforded a white precipitate, which was filtered, thoroughly washed with chloroform, methanol and Hexane and dried under vacuum. Yield 0.345 g (74%). Anal. calcd for $C_{27}H_{26}N_6O_7$: C, 59.32; H, 4.79; N, 15.38. Found C, 59.14; H, 4.86; N, 15.09. *m/z* (ESI- MS, $[1+H]^+$), 547.19 (calcd. 547.19). To obtain the single conformer, ^{1}H NMR measurement was performed by dissolving the solid in [D_6] DMSO in presence of 3 equiv. of LiOH•H_2O. ^{1}H-NMR (500 MHz, [D_6]DMSO, 25 °C): δ = 8.48 (s, 1 H, =CH); 8.20 (s, 2 H, =CH); 7.26- 7.10 (m, 6 H, Ar); 6.76- 6.66 (m, 6 H, Ar); 2.69, 2.58 (dd, 4 H, -CH_2). IR (KBr, cm^{-1}): υ(-OH) 3405, υ(–NH) 3200, υ(C=O) 1661, 1621 (s), υ(C=N) 1526 (s). UV-Vis. [DMF, λ_{max}, nm (ε, M^{-1} cm^{-1})]: 322 (40000), coupled 292, 281 (59000).

Synthesis of Isomer 2: It was synthesized following the similar procedure described for **1**, using 4-hydroxybenzaldehyde instead of 2-hydroxybenzaldehyde. Yield 0.330 g (71%). Anal. calcd for $C_{27}H_{26}N_6O_7$: C, 59.32; H, 4.79; N, 15.38. Found C, 59.26; H, 4.64; N, 15.21. *m/z* (ESI- MS, $[1+H]^+$),

547.19 (calcd. 547.19). ^{1}H-NMR (500 MHz, [D_6] DMSO): δ =8.29(s, 1 H, =CH); 8.04 (s, 1 H, =CH); 7.87 (s, 1 H, =CH); 7.43 (s, 6 H, Ar); 6.74 (s, 6 H, Ar); 2.70 (d, 4 H, -CH_2). IR (KBr, cm^{-1}): υ(–NH) 3247, υ(C=O) 1661- 1606 (s), υ(C=N) 1513 (s). UV-vis. [DMF, λ_{max}, nm (ε, M^{-1} cm^{-1})]: 310 (58500), 295 (70500).

Synthesis of 1/Li^+/Cd(II) (non-sonicated) complex: Isomer 1 (5.0 mg, 9 mmol) was dissolved in DMF (0.6 mL) in a vial followed by the deprotonation with LiOH•H_2O (1.15 mg, 27 mmol) resulted a pale yellow color clear solution. The freshly prepared $Cd(OAc)_2$ (3.66 mg, 13 mmol) solution in DMF (0.4 mL) was added to deprotonated solution of 1 and the resulting transparent clear yellow color mixture solution left for stirring for 5 hours. The resulting solution was evaporated under reduced pressure till complete dry. The ensuing solid was washed with excess water, methanol and diethyl ether to remove salts and other impurity formed during course of reaction. Yield 74%. Anal. Calc. for: [$LiCd(C_{27}H_{23}N_6O_7)$].13H_2O: C, 36.07; H, 5.49; N, 9.35. Found C, 36.06; H, 5.45; N, 9.41. ESI−MS *m/z*: [$Cd(C_{27}H_{25}N_6O_7)]^+$, 659.08 (calc. 658.08). IR (KBr, cm^{-1}) υ(C=O) 1659, 1612, 1546; υ(C=N) 1468.

Note: The details of synthesis and complete gel complex (after ultrasonication product) characterization inserted in main text.

Synthesis of 1/Li^+/Zn(II) complex: To a methanolic suspension of isomer **1** (0.100 g, 0.183 mmol) LiOH was added (0.023 g, 0.549 mmol) at constant stirring which led to a clear solution. Methanolic solution of $Zn(OAc)_2$ (0.060 g, 0.274 mmol) was added to above stirring mixture which immediately produced the pale yellow precipitate. Further this solution was filtered after 6 hours stirring at room temperature and residue was re-crystallized by DMF-water layering method. Light yellow colored green fluorescent crystals were obtained within 10 days. Yield ~45%. Anal. Calc. for: [$Zn_3(C_{27}H_{23}N_6O_7)_2$].12$H_2O$: C, 43.36; H, 4.72; N, 11.24. Found C, 43.23; H, 4.68; N, 11.54. ESI−MS *m/z*: [$Zn_3(C_{27}H_{22}N_6O_7)_2H]^-$, 1281.09 (calc. 1281.10). IR (KBr, cm^{-1}) υ(C=O) 1643, 1614, 1538; υ(C=N) 1468. Weight loss as per TGA: 15.66 % (calc. for: 13 H_2O + CH_3OH 15.63%).

Note: Use of KOH and $Zn(ClO_4)_2$ or filtrate or DMF also produce similar crystal with equal crystallographic parameter.

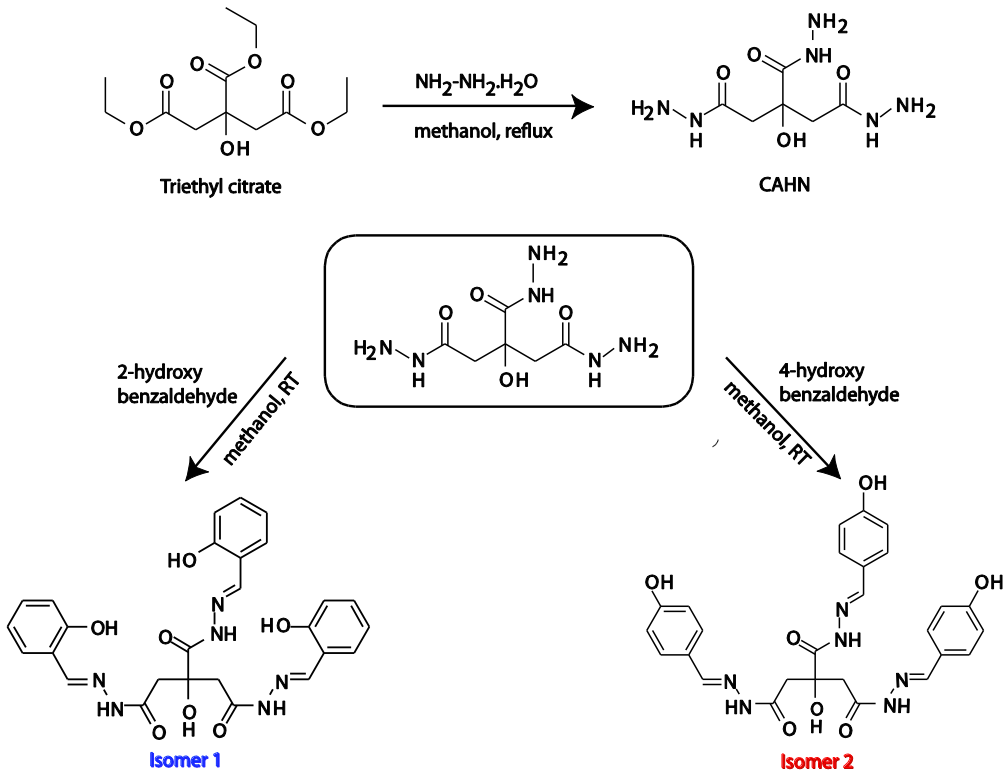

Scheme S1: Synthetic scheme for structural (positional) isomers **1** and **2** along with precursor compound citric hydrazone (CAHN).

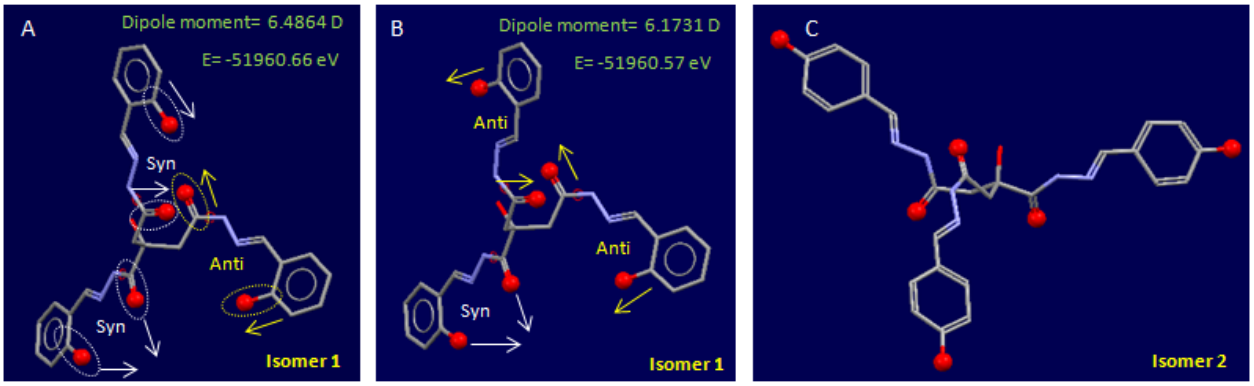

Scheme S2: DFT optimized structures of (A) *Syn-Syn-Anti* and (B) *Anti-Anti-Syn* conformers of isomer 1 with their dipole moments and energies, respectively. ^{1}H NMR well demonstrate these two conformers in 2:3 ratio and (C) model of corresponding regioisomer 2 with no conformer possibilities which was also observed experimentally in ^{1}H NMR (*vide infra*).

***Syn* and *Anti* conformation notations:** The citric acid based isomer 1 has three arms for metal binding and each arm has their own orientation in space. Let's consider one arm of ligand 1- If the phenolic –OH and -C=O are lying in same direction then the notation will be *syn*. If both the –OH and -C=O prefer to stay in opposite direction to each other then the conformation will be *anti*. Thus, we assigned these

notations for the entire three arms for instance *anti*/*anti*/*syn.* For further detail see- B. Levranda, W. Fiebera, J. M. Lehn and A. Herrmann, *Helv. Chim. Acta*, 2007, **90**, 2281.

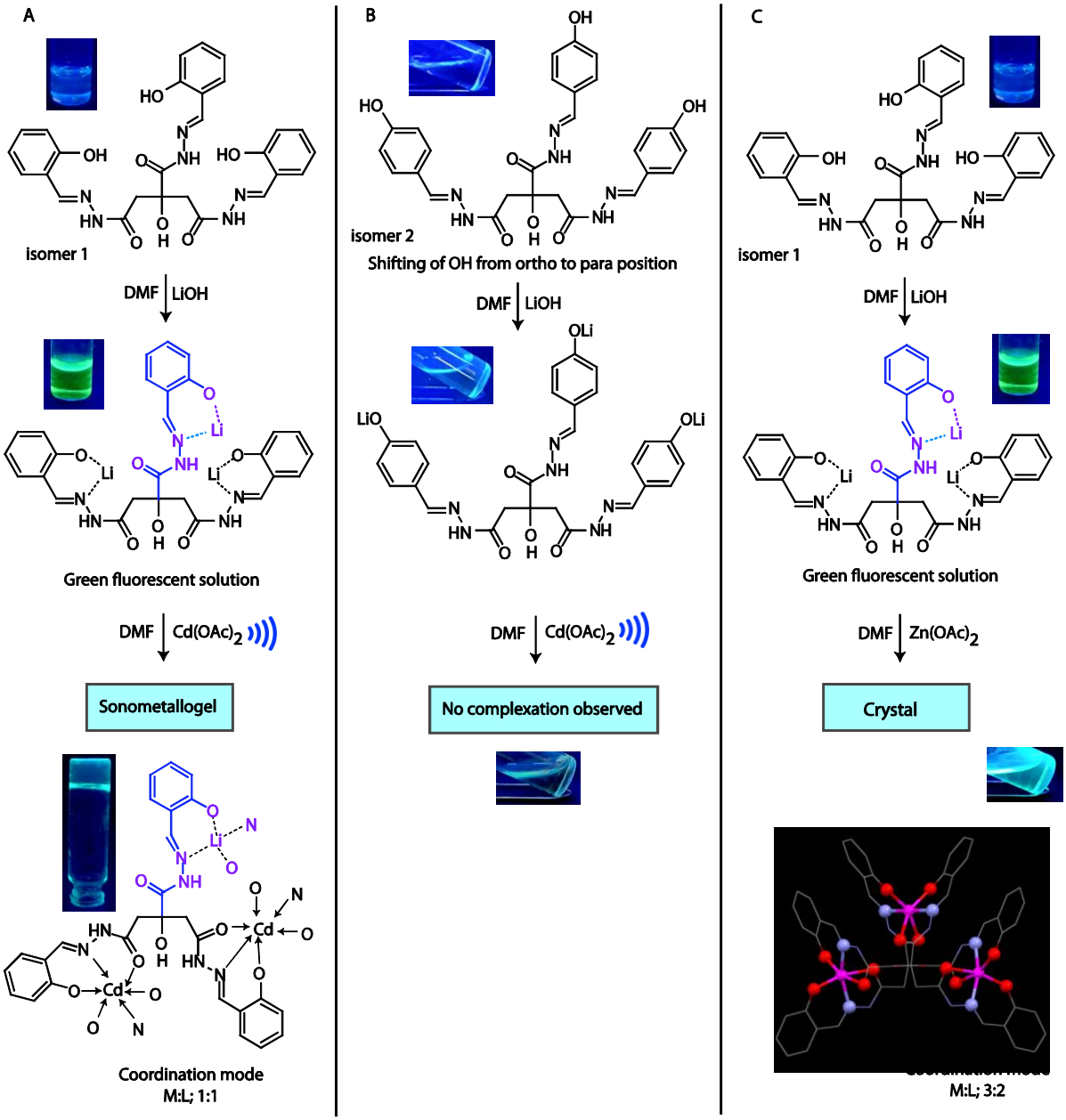

Scheme S3: A comparative stepwise synthetic scheme along with fluorescence change (A) structural (positional) isomers **1** produce fluorescent metallogel upon reaction with LiOH and $Cd(OAc)_2$ in DMF under ultrasonication. The structure of metallogelator and xerogel could derive from various instrumental techniques. (B) regioisomer 2 produces non fluorescent solution under similar reaction conditions to isomer 1. (C) Isomer 1 produces fluorescent crystals when Cd(II) is replaced by Zn(II). The crystal structure and it's solution studies shows the binding mode and ration of metal-ligand different from Cd(II)-gel structure, it is probably due structural dissimilarity with Cd(II) and Zn(II) produces two different entity *viz*, gel and crystal .

Table S1. The characterization data for 1/Zn(II) crystal and 1/Cd(II) gel tabulated for comparison which clearly indicates the two different structures in Zn(II) crystal and Cd(II) gel.

S.N.	Experiment	1/Zn(II) (crystal)	1/Cd(II) (xerogel)
1.	IR (cm^{-1})	υ(C=O) 1643, 1614, 1538, υ(C=N) 1468. (Figure S11)	υ(C=O) 1661, 1610, 1539, υ(C=O) 1470. (Figure S11)
2.	UV-vis (nm)	376	378
3.	Job's plot (M:L)	3:2 (Figure S12)	1:1 (Figure S12)
4.	ESI-Mass (*m/z*)	1281.09 (Figure S13)	659.08 (Figure S13)
5.	Conductance ($ohm^{-1}cm^2mol^{-1}$, DMF)	12	15
6.	CHN analysis	$Zn_3(C_{27}H_{23}N_6O_7)_2].12H_2O$: Calcd C, 43.36; H, 4.72; N, 11.24. Found C, 43.23; H, 4.68; N, 11.54.	$[LiCd(C_{27}H_{23}N_6O_7)].6H_2O$: Calcd C, 41.96; H, 4.56; N, 10.88. Found C, 41.78; H, 4.63; N, 10.84.
7.	Weight loss as per TGA:	15.66 % (calc. $13H_2O+CH_3OH$ 15.63 %) remaining two step degradation corresponding to ligand (Fig. S14)	5.39 % (calc. for $2H_2O$ 5.47 %); 10.85 % (calc. for DMF 11.09 %) and 14.06, 13.75, 22.88 % are corresponding to various kind of degradation of ligand (Fig S14)
5.	Fluorescence spectra (nm)	470	468
6.	Effect of ultrasonication		
	a) UV-vis spectra	No change	Demetallation & Remetallation observed
	b) Fluorescence spectra	No change	Demetallation & Remetallation observed
7.	Molecular formula	$[(C_{27}H_{23}N_6O_7)_2Zn_3]$	$[C_{27}H_{24}N_6O_7Cd]$
8.	Nature of molecule	Trinuclear complex	Coordination polymer
9.	Reference		J. D. Ranford, J. J. Vittal and Y. M. Wang, *Inorg. Chem.*, 1998, **37**, 1226

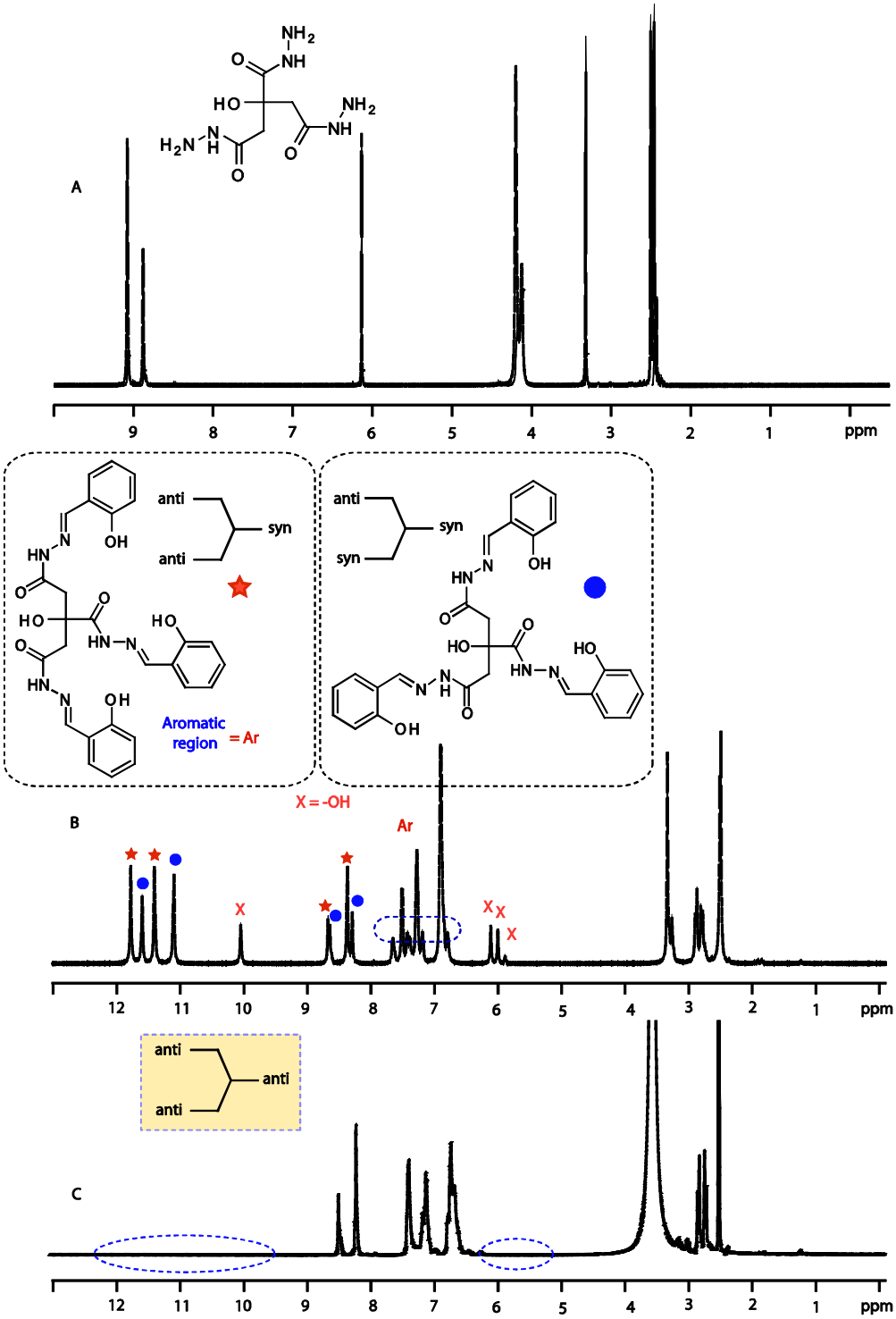

Fig. S1 ^{1}H NMR spectra (500 MHz, DMSO-d_6, 298 K) for (A) precursor compound citric hydrazone (CAHN), (B) isomer **1**, where sketch diagram of two plausible conformers *anti-anti-syn* and *syn-anti-syn* in the ratio of 3:2 are pasted along with their corresponding asterisk and oval shape symbol label and (C) two plausible conformers *anti-anti-syn* and *syn-anti-syn* of isomer 1 converted into single conformer *anti-anti-anti* upon treatment with LiOH. The labile protons regions –NH and –OH were deprotonated after treatment with LiOH (deprotonated region shown by blue dotted circle).

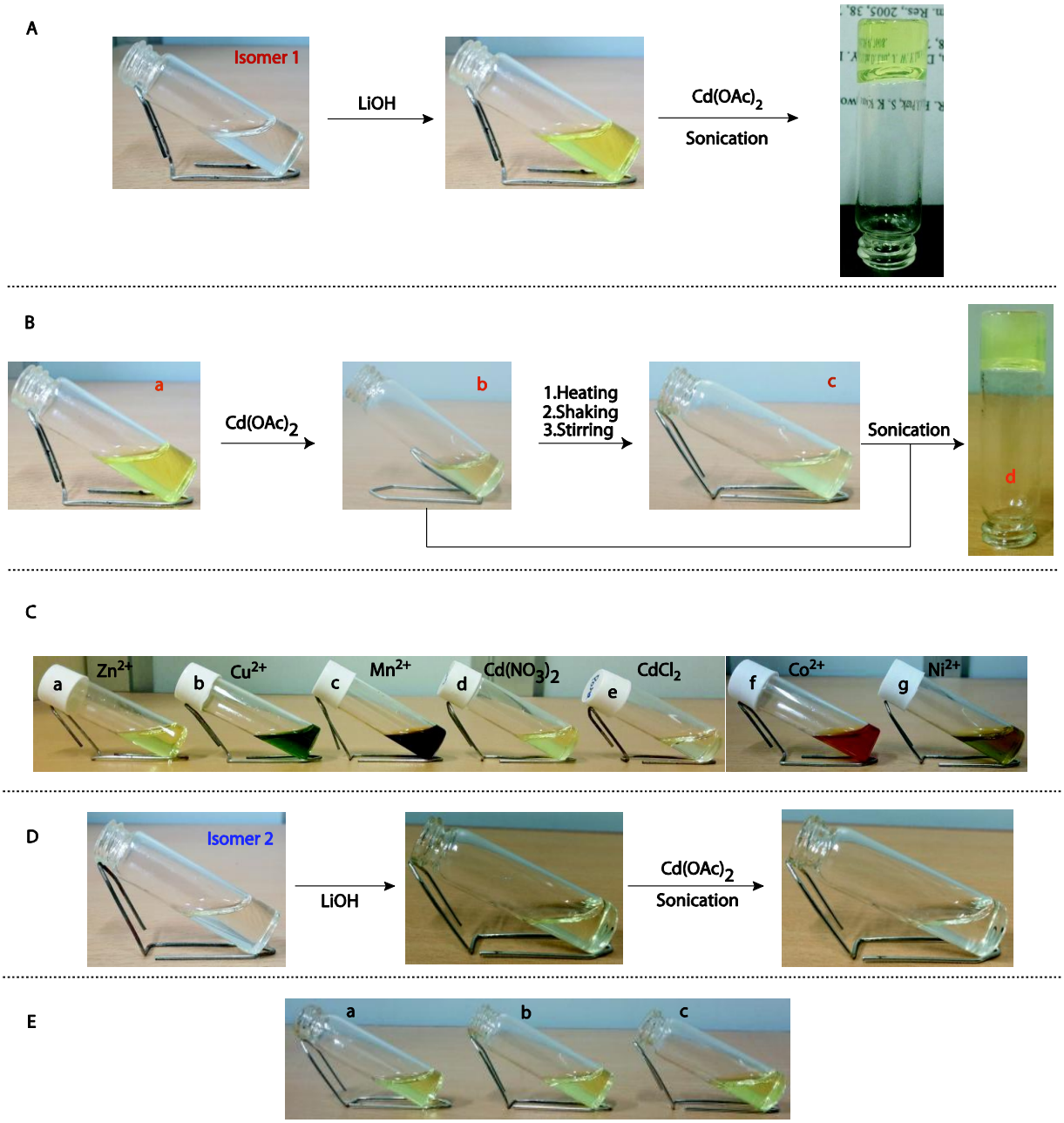

Fig. S2 Photographs shows stepwise visual changes under visible light in DMF (**A**) Isomer **1** forms metallogel in presence of LiOH and $Cd(OAc)_2$ upon brief sonication, (**B**) Sonication is the basic need for gelation and it can not be substituted by other tested conventional methods like heating, shaking or stirring, (**C**) Absence of gelation with other metal salts a) $Zn(OAc)_2$, b) $Cu(OAc)_2$, c) $Mn(OAc)_2$, d) $Cd(NO_3)_2$, e) $CdCl_2$, f) $Co(OAc)_2$, g) $Ni(OAc)_2$, (**D**) Gelation test of isomer **2**+LiOH with $Cd(OAc)_2$ under similar conditions to isomer **1** shows transparent solution instead of gel indicating the importance of position of –OH in gelation. (**E**) Isomer **1** in presence of NaOH, KOH, CsOH (a, b and c respectively) and $Cd(OAc)_2$ followed by sonication under similar conditions to A shows the clear solution.

Table S2. Gelation ability of **Isomer 1** in DMF with variations of alkali base and metal salts.

Metal salt	LiOH	NaOH	KOH	CsOH
$Zn(OAc)_2 \cdot 2H_2O$	S	S	S	S
$Cu(OAc)_2 \cdot H_2O$	SP	SP	SP	SP
$Ni(OAc)_2 \cdot 4H_2O$	S	S	S	S
$Co(OAc)_2 \cdot 4H_2O$	S	S	S	S
$Mn(OAc)_2.H_2O$	S	S	S	S
$Cd(OAc)_2 \cdot 2H_2O$	**G**	S	S	S
$Cd(NO_3)_2.6H_2O$	S	S	S	S
$CdCl_2$	S	S	S	S
$Zn(NO_3)_2.6H_2O$	S	S	S	S
$Zn(ClO_4)_2.6H_2O$	S	S	S	S

S = Soluble, G = Gel, SP = Suspension

NOTE: Isomer **2** forms clear transparent solution instead of gel under similar conditions to isomer **1**.

Table S3. Gelation ability of other solvents in isomer **1** along with LiOH and $Cd(OAc)_2$.[#]

Solvent	Solubility/Gelation ability
DMF	**G**
DMSO	SP
Methanol	SP
Ethanol	SP
Water	SP
Acetone	I
Acetonitrile	I
Ethyl Acetate	I
DCM	I
THF	I
Chloroform	I
1,4-Dioxane	I
Hexane	I

[#]**SP =** suspension**, I =** Insoluble, **G**= Gel

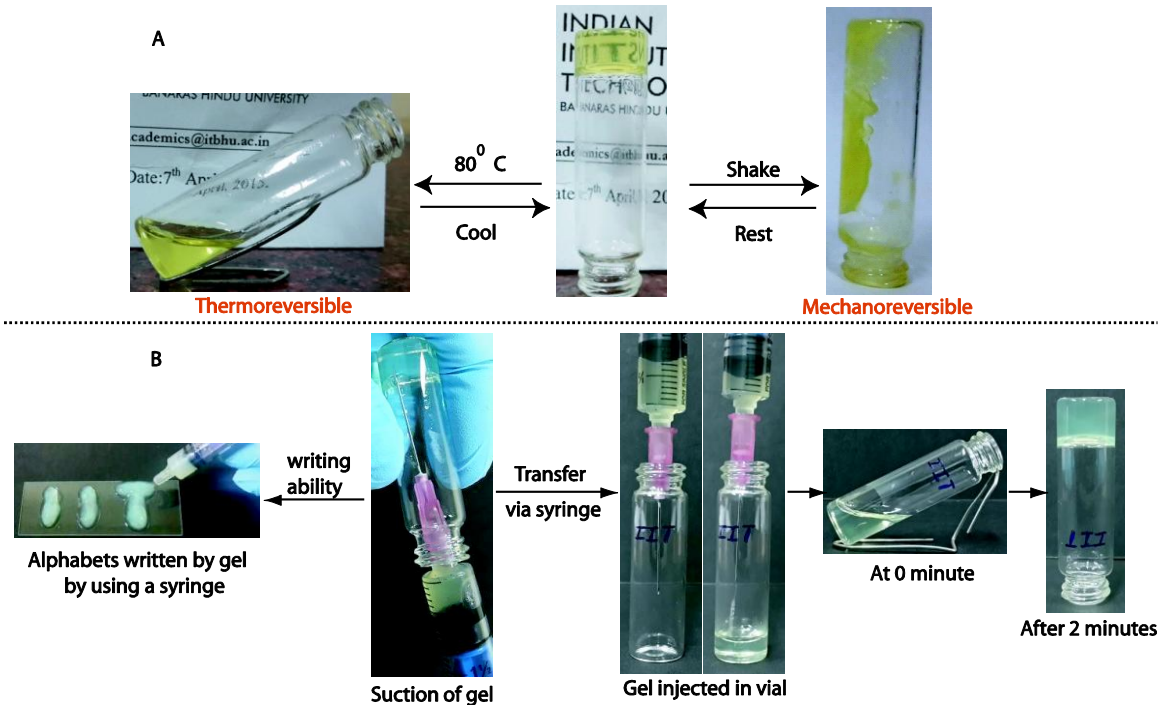

Fig. S3 A pictorial representation of various kinds of physical properties in one gel ('*many in one*') like (**A**) Thermal and mechanical reversible property, (**B**) can be used for writing purpose and also can be transferred by injecting from one vial to another vial with the help of syringe.

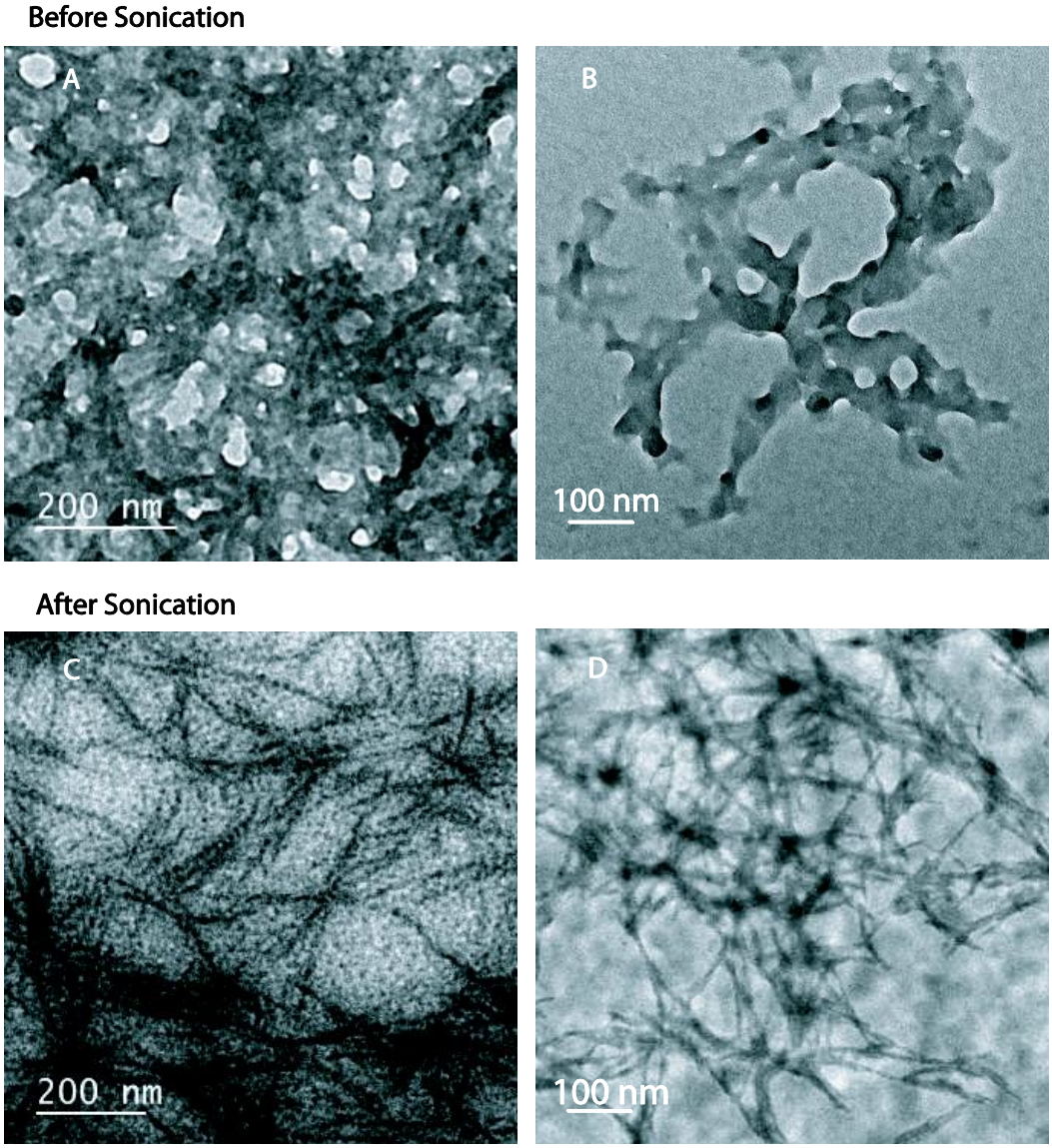

Fig. S4 TEM images of diluted samples ($1x10^{-5}$ M) (**A**, **B**) before sonication reveals non directional wrecked aggregate growth at two different magnifications and (**C**, **D**) upon sonication wrecked aggregate converted into well ordered, directional, long range nano-fibers with average diameter of ~20 nm.

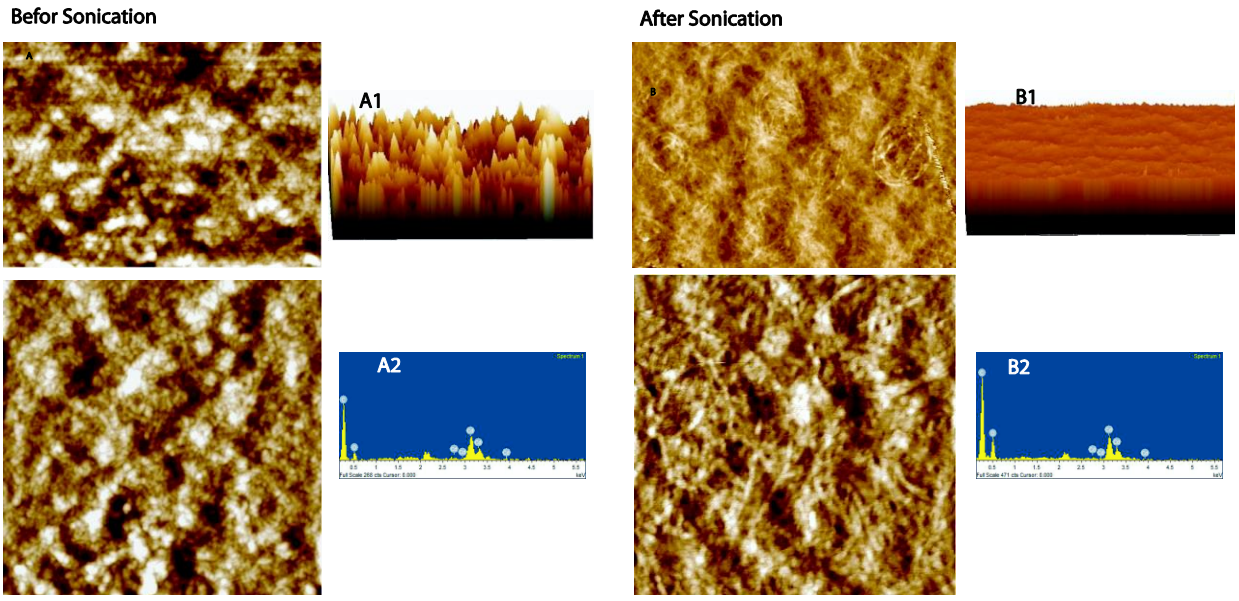

Fig. S5 AFM images of diluted samples ($1x10^{-5}$ M) (**A**) Before Sonicated, sample exhibiting wrecked aggregate appearance with (**A1**) rough surface morphology, and (**B**) Sonicated diluted gel, showing nano-fibrous morphology with (**B1**) almost smooth surface structure appeared due to the uniform nano fiber formation. (**A2, B2**) EDAX plot shows that the elemental profile is quite similar before and after sonication.

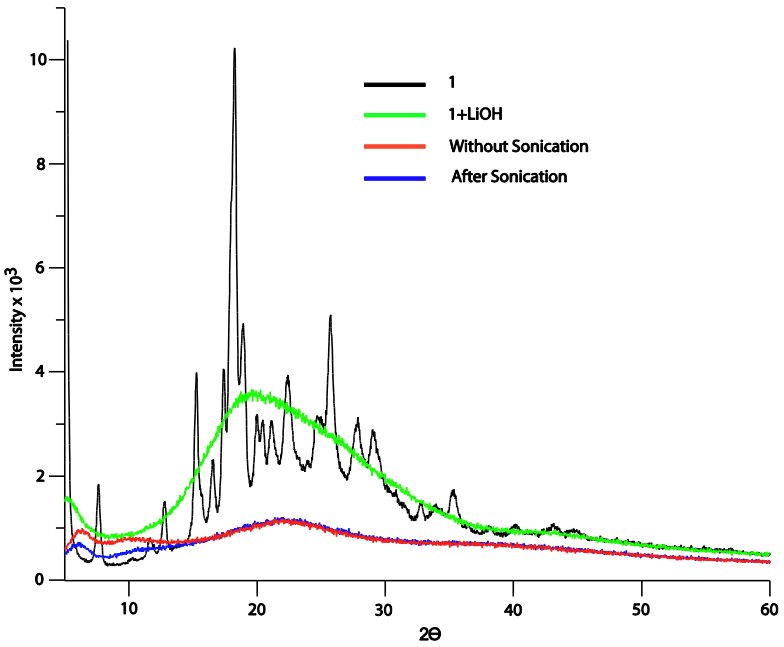

Fig. S6 Powder X-ray diffraction pattern of isomer **1** (black line), 1/3LiOH (green line), 1/3LiOH/$Cd(OAc)_2$ (blue line; before sonication) and xerogel (red line) indicating ligand losses its crystalline nature upon deprotonation and completely amorphous upon complexation and gelation (xerogel).

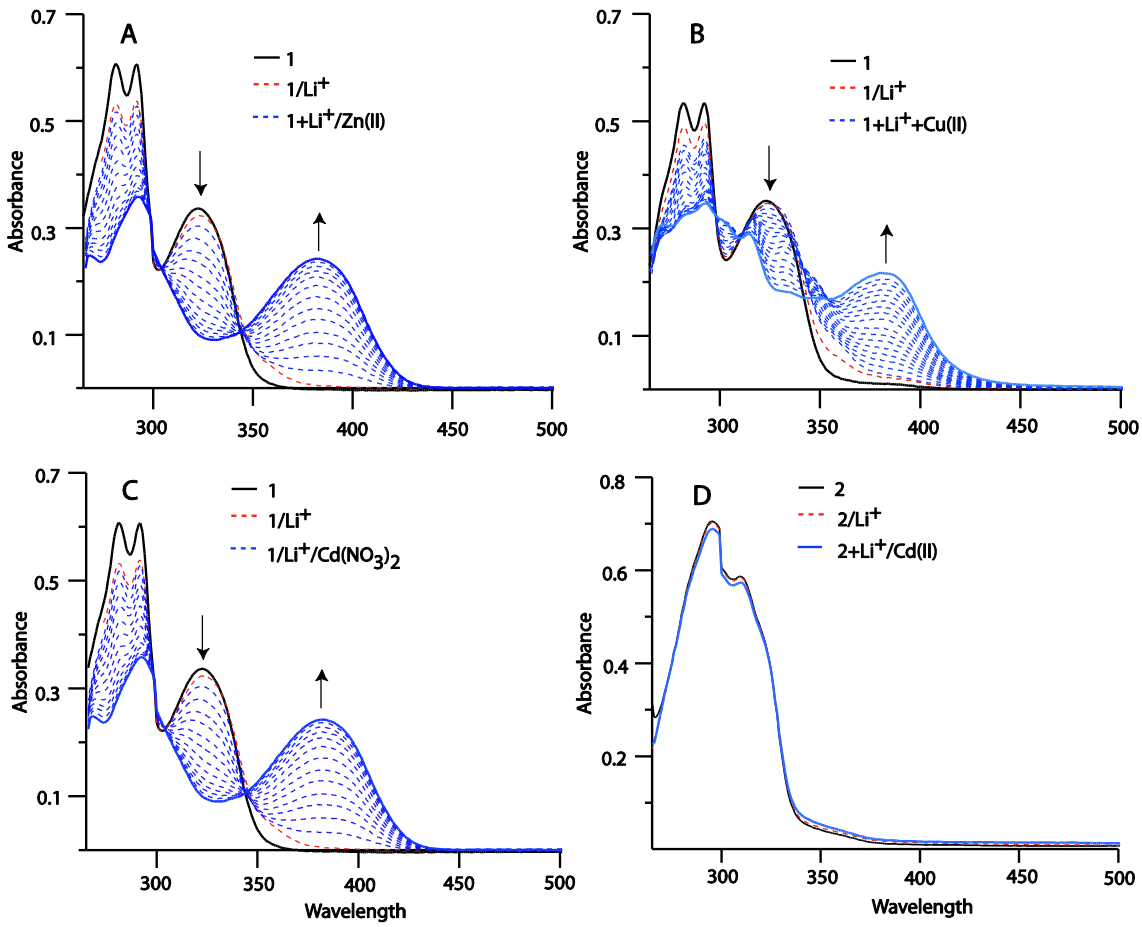

Fig. S7 UV-vis titrations in DMF (**A**) ligand **1** (black line; λ_{max} 322 nm; $1x10^{-5}$ M), deprotonation with LiOH (3 equiv., red line) and upon aliquot addition of $Zn(OAc)_2$ (blue line) band corresponding to ligand diminishes and a new band appears at 378 nm, simultaneously through isobestic point; (**B**) similar titration experiment with $Cu(OAc)_2$, (**C**) with $Cd(NO_3)_2$; (**D**) Sequential mixing of isomer 2 with LiOH and $Cd(OAc)_2$ shows no significant change highlighting positional importance of position of –OH towards metal binding.

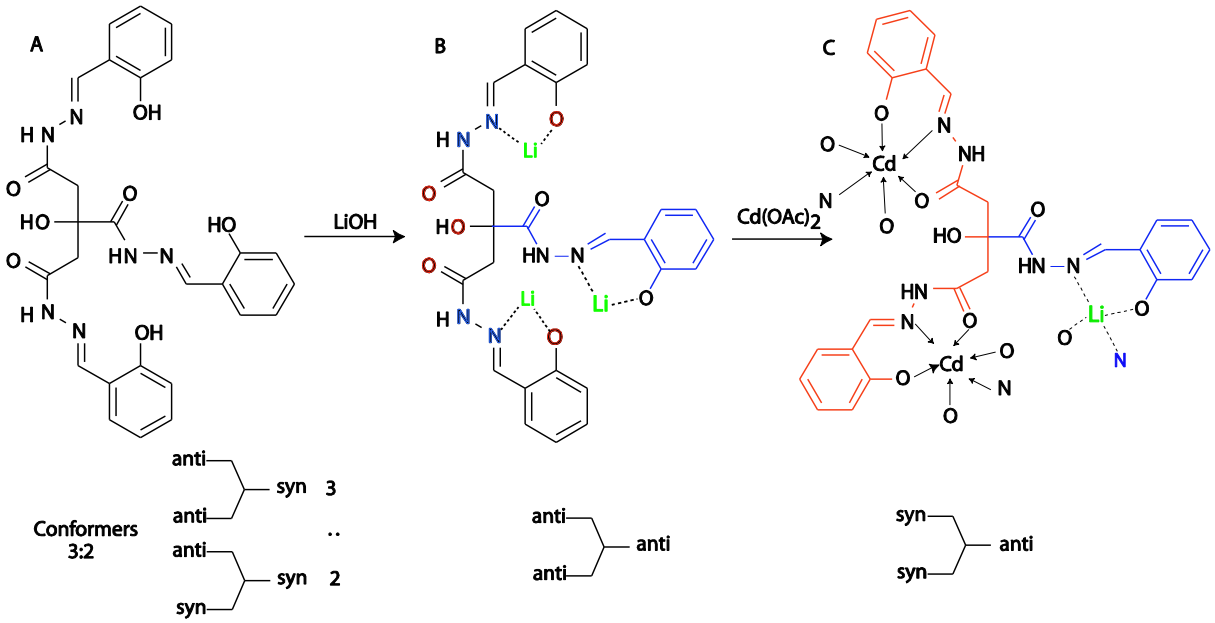

Fig. S8 Sketch diagram shows the possibility of conformational changes in **1** at various stage (**A**) ligand 1 in two possible conformations *anti-anti-syn* and *anti-syn-syn*, (**B**) upon LiOH deprotonation (Li^+ interaction) of ligand changed into single conformation *anti-anti-anti*, (**C**) upon Cd^{2+} chelation again changes into *syn-syn-anti* conformation which has been justified by IR, UV-vis, fluorescence and NMR experiments.

Explanation: All the possible conformations of **1** have been derived from IR, ^{1}H NMR, UV-vis and fluorescence (**A**) IR spectrum of isomer 1 shows characteristic bands at 3405, 1661-1621 and 1526 cm^{-1} corresponding to υ(OH), υ(C=O), υ(C=N), respectively; (**B**) Upon addition of Li^+, there is no significant change observed in peaks respective to C=O, but disappearance of band corresponding to υ(OH) along with slight shifting in υ(C=N) band to 1537 cm^{-1} suggests deprotonation and weak interaction of Li^+ with C=N; (**C**) Addition of Cd^{2+} originate the shift in bands corresponding to υ(C=O) and υ(C=N) up to 1610, 1539 and 1470 cm^{-1} respectively along with a small un-shifted band corresponding to υ(C=O) at 1661 cm^{-1} suggests one C=O is remain free from metal ion binding. Thus, it can be concluded that the eventual possible conformation is may be *syn-syn-anti* conformer.

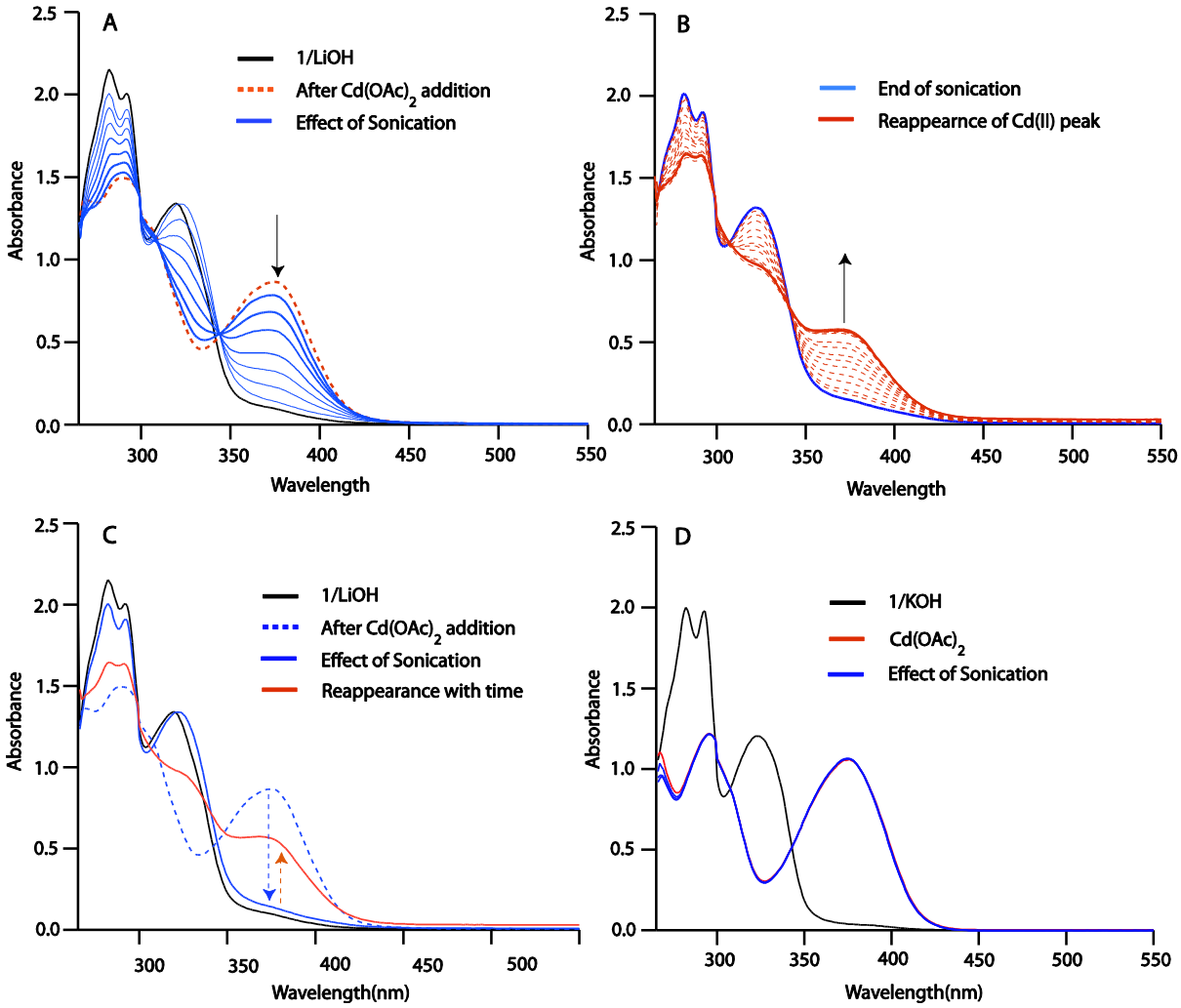

Fig. S9 Effect of sonication monitored in UV-vis experiment of deprotonated **1** (0.5 x 10^{-4} M, DMF) (**A**) Band corresponding to 1/LiOH/$Cd(OAc)_2$ decreases and dynamically converted into band corresponding to ligand **1** upon brief sonication with 30 seconds interval suggests that there must be demetallation; (**B**) Again recover the band corresponding to Cd(II)-complex with resting time approximately 5 minutes, (**C**) Comparative decrease in absorbance with sonication and reappearance of peak with time indicates the demetallation with sonication and remetallation with resting, while (**D**) shows no effect of sonication with non gelling combinations 1/KOH/$Cd(OAc)_2$ indicates role of Li^+ in gelation.

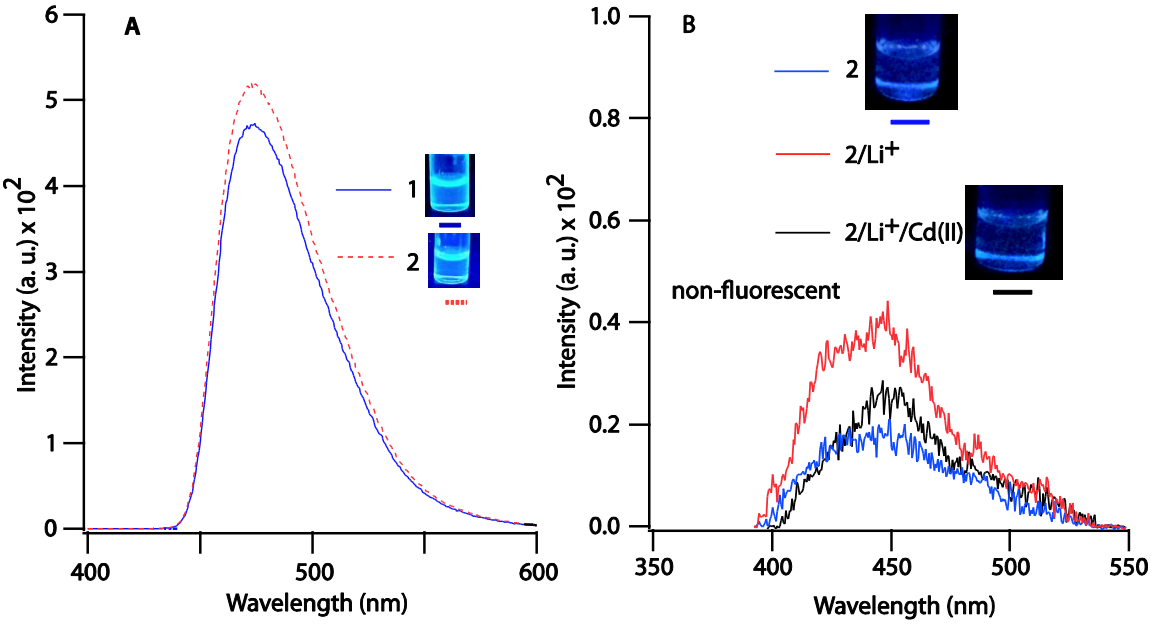

Fig. S10 Effect of sonication on flourescence spectra ($2x10^{-2}$ M, gelation concentration), where, blue line before sonication and red dotted line after sonication. There is no effect of sonication on the emission intensity of non gelling combinations (**A**) 1/KOH/$Cd(OAc)_2$ while Flourescence of isomer **2** ($1x10^{-4}$ M, λ_{ex} = 295 or 309 or 321 nm) upon addition of LiOH and $Cd(OAc)_2$ indicating the non-fluorescent nature because of absence of CHEF which highlight the importance of position of –OH.

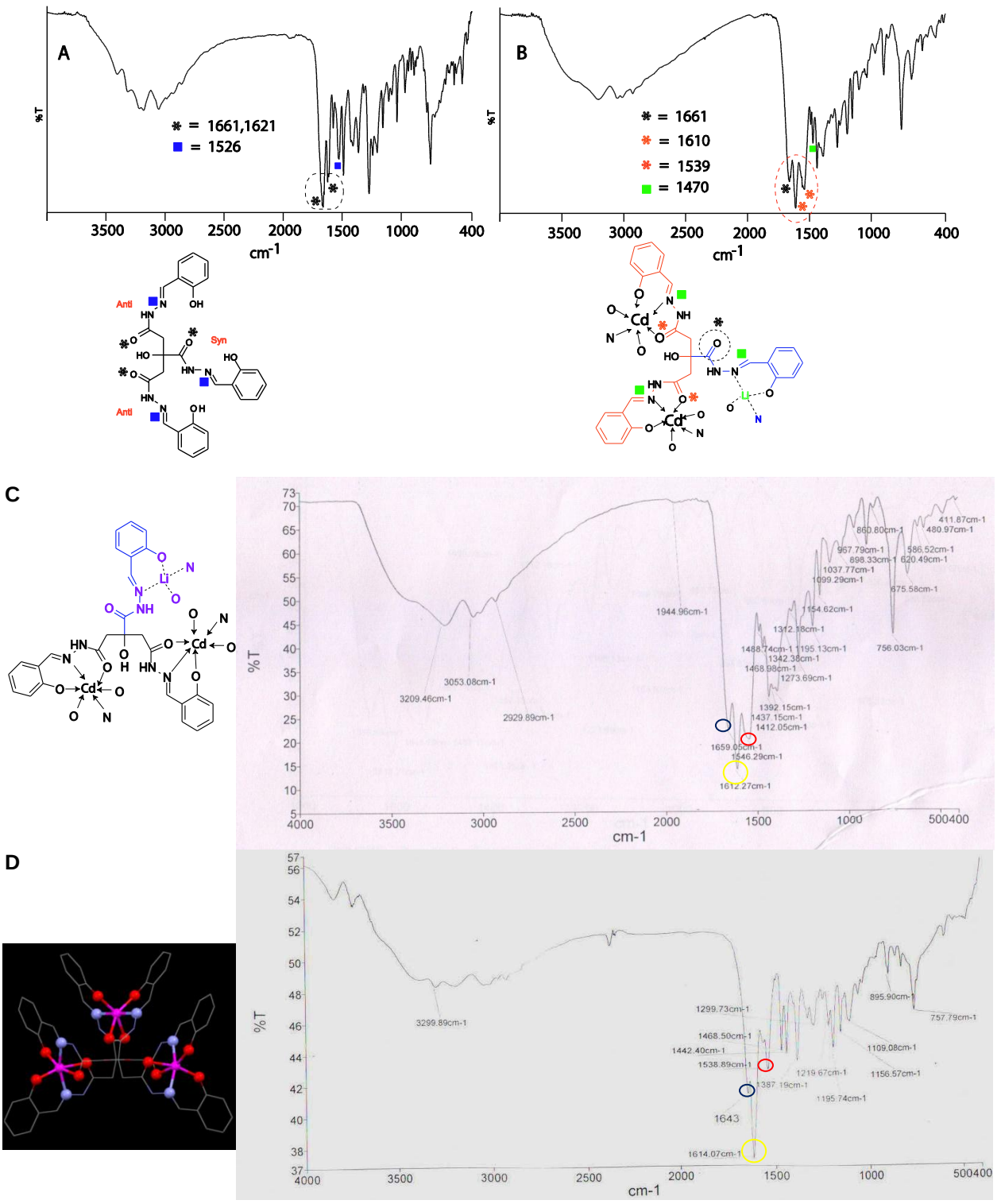

Fig. S11 FTIR spectra for (**A**) Isomer **1** illustrate υC=O at 1661, 1621 cm^{-1} and C=N at 1526 cm^{-1}, (**B**) xerogel (1/Li^{+}/Cd(II)) indicating the down shift of υC=O at 1610 and 1539 cm^{-1} and C=N at 1470 cm^{-1} along with unshifted peak related to C=O at 1661 cm^{-1}, which supports the binding mode of ligand with Cd^{II} and Li^{+}, (**C**) Non-sonicated sample (1/Li^{+}/Cd(II)) shows no change in the peak position with respect to

xerogel (important peaks are pointed out with colored circles), (**D**) Crystals of 1/Li^{+}/Zn(II) supports the binding mode as observed in crystal structure; All the three –C=O are significantly shifted indicates the involvement in binding with Zn(II) unlike Cd(II) in xerogel.

Note: Crystal structure and IR of 1/Li^{+}/Zn(II) indirectly supports one arm of isomer 1 free from Cd(II) binding. Further support obtained from Job's plot and ESI-mass spectra (*vide infra*). The asymmetric unit repetition found to be in ESI-mass spectra also supports the polymeric nature of structure involved in metallogel formation with Cd(II) while absent in case of Zn(II) crystals mass.

A

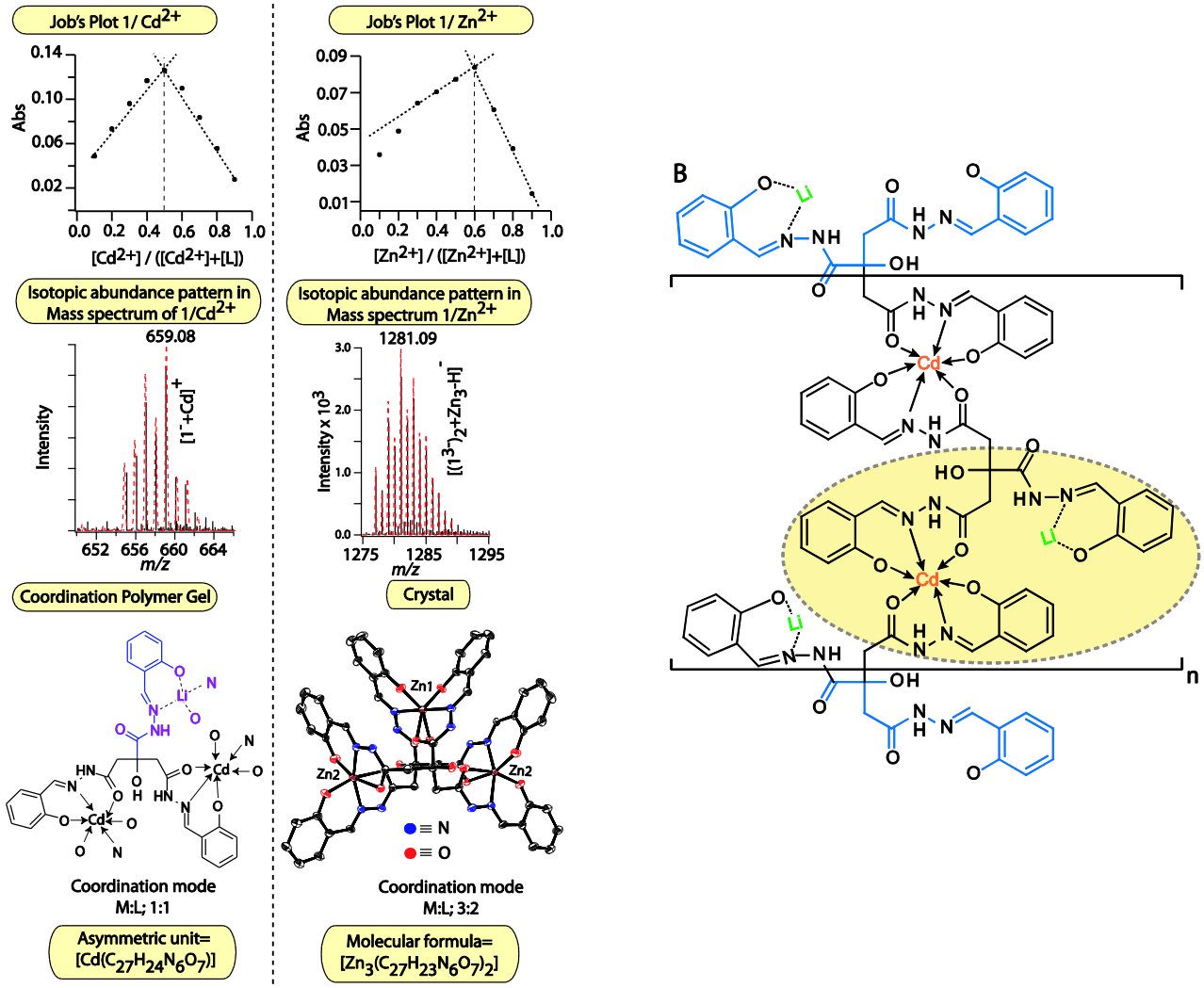

Fig. S12 (**A**) Comparative profile for Job's plot performed in DMF for (left) LiOH deprotonated **1** *vs.* $Cd(OAc)_2$ showing 1:1 stoichiometry, [Cd^{II}]/[Cd^{II}]+[1] *vs.* absorbance monitored at 378 nm and (right) LiOH deprotonated 1 *vs.* $Zn(OAc)_2$ found to be ratio 2:3. ESI-mass and crystal structure well supports the results obtained from Job's plot. (**B**) The structure of complex derived as coordination polymer demonstrated through sketch diagram along with asymmetric unit highlighted through colored circle. Crystal data: $C_{55}H_{90}N_{12}O_{38}Zn_3$, Fw 1723.50, T (K) 293(2), monoclinic, C2/c, a = 17.499(15) A °, b = 22.610(3) A ° , c = 19.196(16) A ° ; β = 105.599, V=7316.0(3) A $^{\circ 3}$, Z=4, F_{calcd}=1.565 Mgm-3, μ=1.079 mm^{-1}, reflections collected 8013,

independent 5197, R1=0.1025, wR2=0.2907 [I > 2σ(I)]; R1 = 0.1338, wR2 = 0.3597 (all data), GOF = 1.209. CCDC number 1524168.

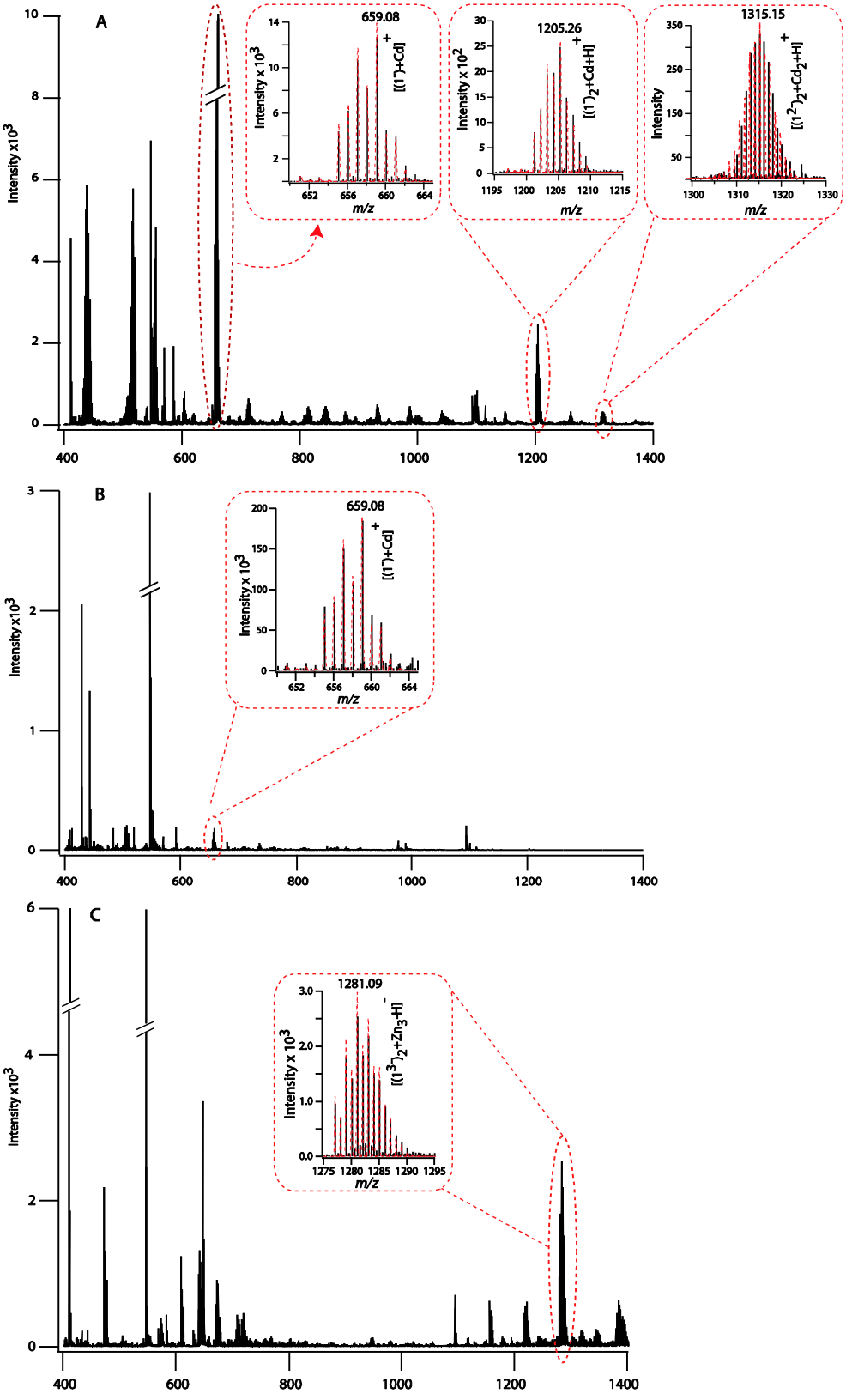

Fig. S13 ESI-MS (DMF) spectra of (**A**) diluted metallogel shows the molecular ion peak of asymmetric unit *m/z,* $[1+Cd^{II}+H]^+$, 659.08 (calcd. 659.08) with matching profile of isotopic abundance pattern of experimental (black line) and simulated (red dotted), supporting the complex formation is at 1:1 ratio. Further analysis of full spectrum shows the repetition of asymmetric at *m/z* 1315.15 with complete matching of isotopic abundance pattern of experimental (black line) with simulated (red dotted) confirms the coordination polymeric nature of structure involved in sonometallogel formation. **(B)** The mixture of $1/Li^+/Cd(II)$ before sonication exhibits very less intense asymmetric unit molecular ion peak at *m/z,* $[1+Cd^{II}+H]^+$, 659.08 (calcd. 659.08), where isotopic abundance pattern of experimental matches nicely with simulated. Notably, other peaks are absent at higher m/z like 1315.15 which also confirms the role of sonication in stable coordination polymeric complex formation as well as gelation. **(C)** Crystals obtained from $(1/Li^+/Zn(II))$ combination shows the molecular ion peak at *m/z* 1281.09. The isotopic abundance pattern of experimental (black line) also matches nicely with simulated (red dotted line). Notably, there were no peaks observed for any indication of coordination polymeric complex formation which indirectly confirms the coordination polymer formation in sonometallogel.

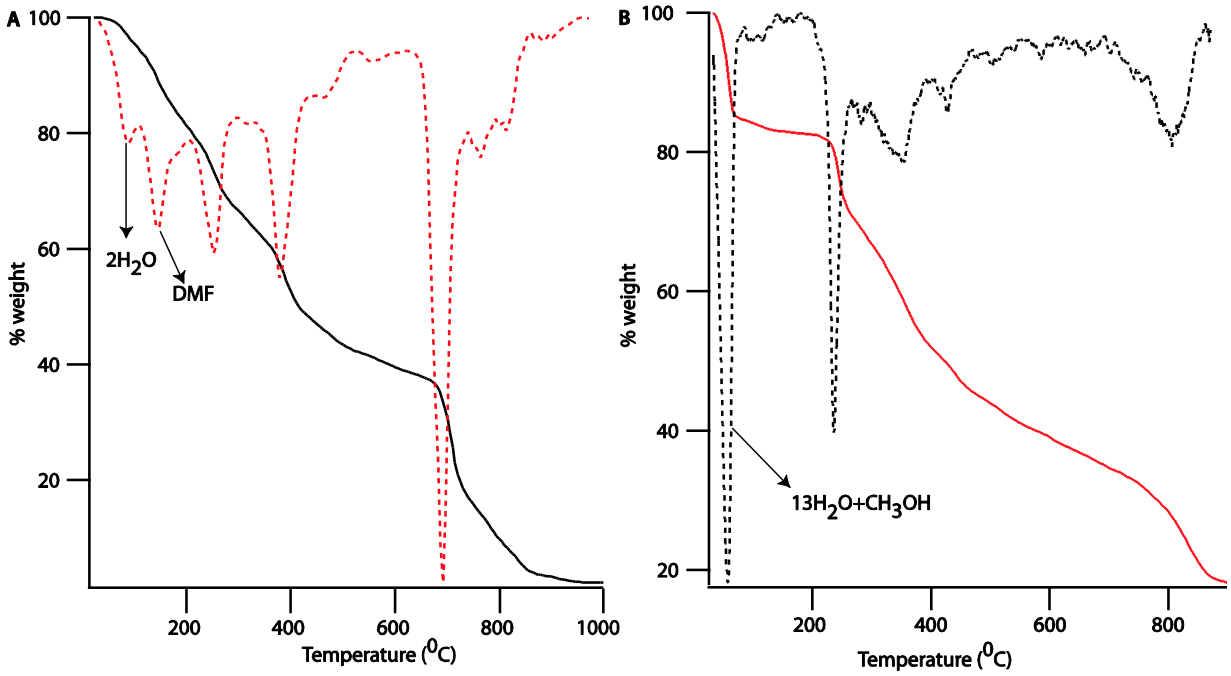

Fig. S14 The Thermo Gravimetric Analysis (TGA) along with derivative plot for (**A**) the isolated compound from xerogel (washed with H_2O to remove extra salts and vacuum dried) shows 5.39% and 10.85% weight loss within the temperature range 45−190 °C, which suggests loss of two lattice water and one DMF molecules, respectively (weight loss as per TGA: 5.39 % (calc. for $2H_2O$ 5.47 %); 10.85 % (calc. for DMF 11.09 %) and 14.06, 13.75, 22.88 % are corresponding to various kind of degradation of ligand) and (**B**) the crystals exhibits weight loss as per TGA: 15.66 % (calc. for: 13 H_2O + CH_3OH 15.63%) which was also observed in crystal structure.

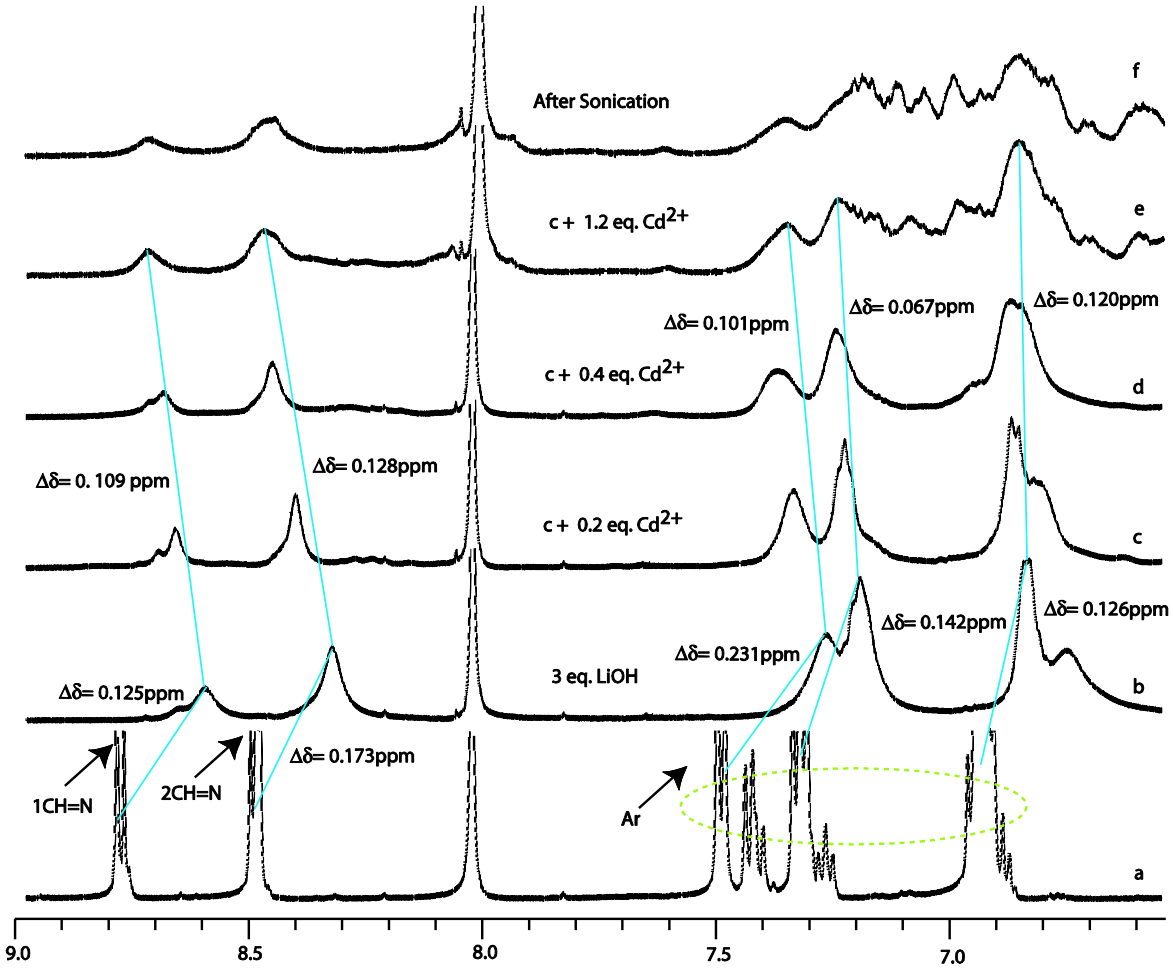

Fig. S15 ^{1}H NMR titration (500 MHz, [D_7]DMF, 25 °C) of (**a**) **1** shows conversion of two plausible conformers *anti-anti-syn* and *syn-anti-syn* into (**b**) single conformer *anti-anti-anti* on addition of 3 eq. LiOH, further addition of $Cd(OAc)_2$ in subsequent steps (**c**), (**d**) and (**e**) shows no significant result other than peak broadening indicate Cd(II) binding in lieu of Li^+, (**f**) with no significant effect of sonication observed. Overall conclusion of NMR titration is broadening of peaks because of the metal binding as well as presence aggregation.

Note: Explanation related to this figure is absent in main text because of lack of conclusion of this experiment except the indication of metal binding and aggregation.

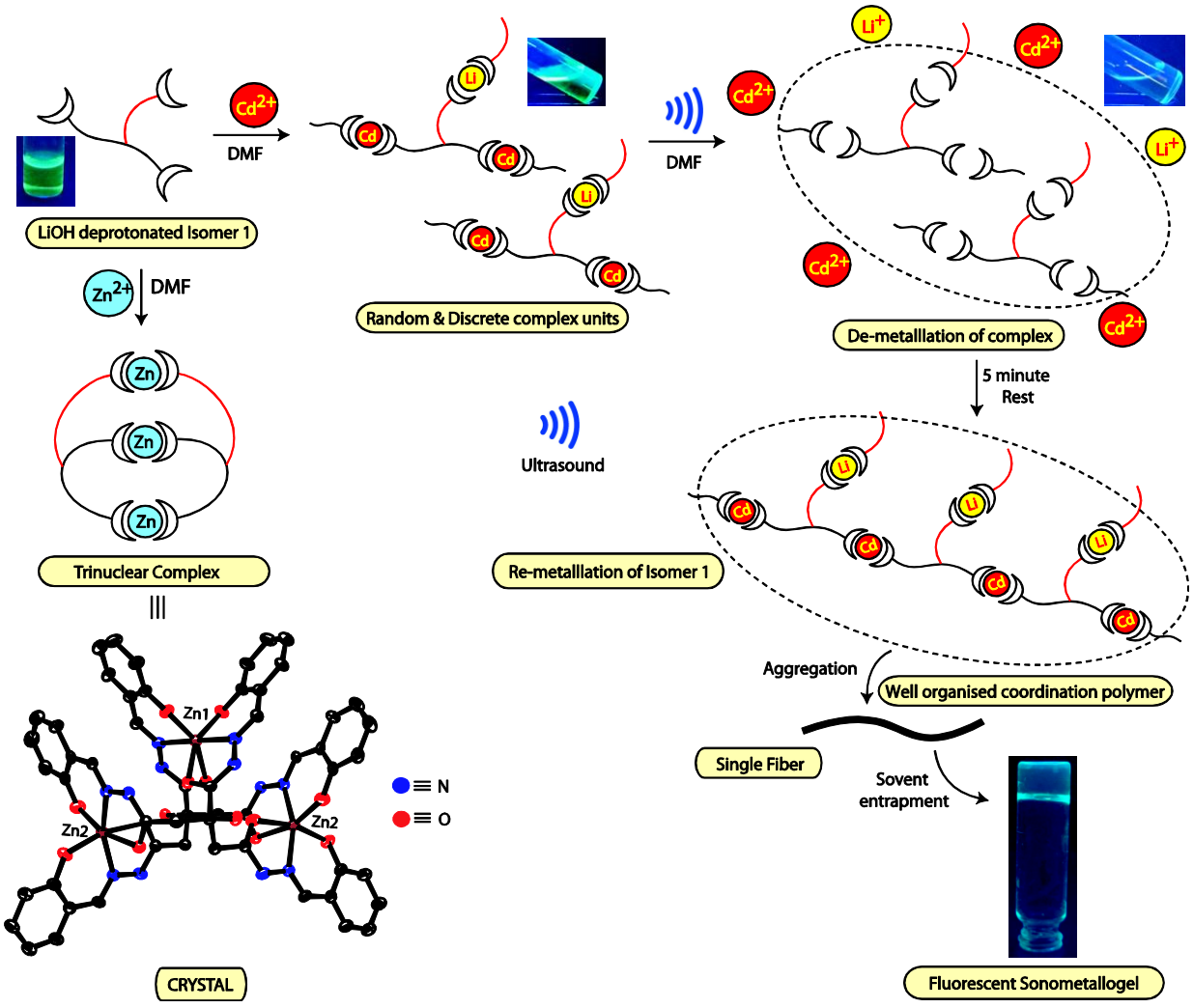

Fig. S16 A model representation of plausible mechanism of the gelation along with structural changes under the influence of ultrasonication, while Zn(II) produces crystal structure. ORTEP diagram with 30% thermal ellipsoid probability and H atoms are removed for clarity.

Explanation: Isomer **1** undergoes conformational change towards more stable *anti-anti-anti* structure in presence of Li^{+}. Fluorescence enhanced upon Cd^{2+} addition to deprotonated **1**, may be due to chelation (CHEF). TEM image at this stage shows the non-directional wrecked aggregate growth. Furthermore, upon brief sonication, de-metallation was evidenced by fluorescence and UV-vis spectroscopy. The fluorescent gel obtained within 5 min resting time. Gelation is due to remetallation/reorganization is well established by UV-vis and fluorescence studies. Based on results obtained from ESI-Mass, Job's plot, IR, TGA, molar conductance, we conclude that final gel structure may be coordination polymer which further undergoes aggregation into nanofibers, facilitates the entrapment of solvent and eventually the fluorescent sonometallogel.